Journal of Applied Polymer Science

Design of Vascular Prostheses by Melt Electrospinning—Structural Characterizations

Olga Mazalevska, Marcin Henryk Struszczyk, Izabella Krucinska
Centre of Advanced Technologies of Human-Friendly Textiles 'Pro Humano Tex,' Department of Material and Commodity Sciences and Textile Metrology, Faculty of Material Technologies and Textile Design, Lodz University of Technology, Lodz 90-924, Poland
Correspondence to: O. Mazalevska (E-mail: olga.mazalewska@p.lodz.pl)

ABSTRACT: The general objective of this research is to use melt electrospinning to design and fabricate semibiodegradable and multilayered fibrous structures that have potential applications for cardiovascular implants, including small-diameter (<6 mm) blood vessels replacements. In the first stage of the study, as described in this article, flat fibrous structures from polypropylene and polylactide polymers were fabricated. The fabrication stage was necessary to determine the effect of the polymers' melt mass flow rate, melt electrospinning processing parameters (as a working distance and spinning voltage) on the resulting fiber diameter and on other physical and structural properties of the fibrous structures. An analysis of the effects of the processing parameters on the fabrication of the fibrous structures and the selection of the appropriate polymers for the final multilayered tubular structure were also performed.
 J. Appl. Polym. Sci. 129: 779–792, 2013

KEYWORDS: biomedical applications; electrospinning; biomaterials

Received 10 August 2012; accepted 9 November 2012; published online 3 December 2012
DOI: 10.1002/app.38818

INTRODUCTION

Large diameter vascular prostheses designed using polyethylene terephthalate and expanded polytetrafluoroethylene are known as the "gold standard" in the vascular prostheses manufacturing process.[1] However, when the diameter of the vascular vessel is small (<6 mm), the success rate of surgical reconstruction is significantly reduced, due to the risk of acute thrombus formation in the short terms and intimal hyperplasia (stenosis) in the long term.[2]

Despite active research on the cardiovascular diseases and vascular surgery, the need for functional, biocompatible and small diameter vascular substitutes is apparent.[3] Electrospinning (using solvent and melt solutions) provides the possibility of obtaining scaffolds characterized by structures with ultrathin fibers, high enhancement of the surface features, large and fully interconnected pores, and tunable mechanical properties.[4–10] Several research efforts have been carried out with the aim of obtaining the appropriate structures for medical applications, such as tissue engineering, using the melt electrospinning method.

Kim et al.[11] fabricated nanofibrous/microfibrous poly-(lactic-*co*-glycolic acid) (PLGA) scaffolds by hybrid electrospinning, which is a combination of solution electrospinning and melt electrospinning that has been used for skin regeneration. The electrospun PLGA nanofibrous/microfiber scaffolds were characterized in terms of their surface morphology, porosity, and mechanical properties, as well as in terms of their capacity for cell attachment and tissue growth.

Sangwon et al.[12] conducted a study on the fabrication of layered vascular scaffolds using an elastomeric and biodegradable 50: 50 poly-(L-lactide-*co*-caprolactone) copolymer using two different approaches: melt spinning and electrospinning. The morphology, mechanical properties, and cell viability of the prototype tubes were examined.

Brown et al.[13] revealed the methods of melt electrospinning polycaprolactone in a direct writing mode. Tubes were designed using 20-μm diameter fibers with controllable micropatterns and mechanical properties.

Ari Karchin et al.[14] described the ability to form tissue engineering scaffolds with aliphatic polyurethane using the melt electrospinning technique.

The aim of this research is to elaborate on a new melt-electrospinning manufacture process for designing small diameter vascular prostheses with a multilayered structure. Melt electrospinning is an attractive method for the production of small diameter, fibrous biomimetic structures with complex porosity for use in tissue engineering and also as a substitute for vascular vessels. The melt electrospinning technique allows for the formation of structures without solvents, which can cause both local and systemic adverse effects. The solvent-free technique

Table I. Melt Temperature of Native PP and PLA Used

	Moplen HP 456J PP	Moplen HP 462R PP	Borflow HL 504FB PP	PLA 4060D	PLA 6201D
Melt temperature (°C)	165	162	167	Amorphous polymer	156

provides the possibility of obtaining scaffold structures characterized by ultrathin fibers, high enhancement of the surface features, large and fully interconnected pores, and controlled mechanical properties. The concept of a multilayered vascular prosthesis design to generate biodegradable structures, the choice of polymers, and the previously mentioned parameters have been presented in a previous publication.[15]

The current stage of study presents the elaboration of flat and one-layered tubular fibrous structures being the part of designed multilayered tubular structures of nonbiodegradable or biodegradable polymers. This part of study is carried out for the optimalization of the melt electrospinning processing parameters as a base for the construction of multilayered structure.

MATERIALS AND METHODS

Materials

Materials Used for Designing the Nonbiodegradable Fibrous Structures. Moplen HP 456J, Moplen HP 462R and Borflow HL 504FB polypropylene (PP) were obtained from Basell Orlen Polyolefins, Poland. The polymers were characterized using melt mass flow rate (MFR) analysis determined according to the ISO 1133 : 2011 Standard. The polymer manufacturer provides MFR values of Moplen HP 456J PP (3.4 g/10 min), Moplen HP 462R PP (25 g/10 min), and Borflow HL 504FB PP (450 g/10 min). The vicat soften temperature (determined according ISO 306/A50 : 2004 Standard by Manufacturer) amounted 154°C for Moplen HP 456J PP and 151°C for Moplen HP 462R PP. Melting temperature (determined according ISO 3146 : 2002 Standard) for Borflow HL 504FB PP is amounted 165°C.

Additionally for each polymer in study used, the melt temperature for native PPs was determined by DSC according the PN-EN ISO 11357 : 2009 Standard. The results are shown in Table I.

Materials Used for Fabricating Biodegradable Fibrous Structures. Two types of polylactide (PLA), amorphous PLA (PLA 4060D) and semicrystalline PLA (PLA 6201D), were purchased from Nature Works LLC. The number average molecular weights for PLA 4060D and PLA 6201D were 87 and 70 kDa, respectively.[16]

According to the specification sheet provided by the polymer manufacturer, the amorphous PLA contains 88.0% L-lactide and 12.0% D-lactide,[17] whereas the semicrystalline PLA contains 98.15% L-lactide and 1.85% D-lactide.[18] The melt temperature of PLA 6201D is ranged 160–170°C (determined according ASTM D3418 : 12 Standard by Manufacturer). Amorphous PLA 4060D shows only seal initiation temperature 80°C (according the ASTM F88 : 2009 Standard).

The same, as in case of PP, the melt temperature for native PLAs was determined by differential scanning calorimetry (DSC) according the PN-EN ISO 11357 : 2009 Standard. The results are shown in Table I. The nonbiodegradable and biodegradable polymers were then used to determine the influence of the MFR and crystallinity index (CI) of the designed structures.

Melt Electrospinning of Flat Structures

Melt electrospinning was performed as previously described.[15] The processing parameters used for the melt electrospinning process are shown in Table II. The fibrous structures were melt electrospun at various temperatures, as shown in Table II. A processing temperature of 300°C was used for the Moplen HP 456J PP polymer to obtain thin fibers, whereas 290 and 280°C were used for the Moplen HP 462R PP and Borflow HL 504FB PP polymers, respectively. The PLA 4060D polymer was treated at 170°C due to its amorphous properties and capacity for quick degradation compared to the semicrystalline PLA 6201D polymer.

Tubular Structures Fabrication

The tubular structures were fabricated using an EH-16H extruder (ZAMAK, Poland) with a specially designed rotating mandrel collector 5 mm in diameter. Figure 1 shows a schematic view of the designed melt electrospinning system for the fabrication of the tubular structures.

The polymers used for the fabrication of the single layered nonbiodegradable and biodegradable tubular structures were chosen based on the selection of the optimal parameters for the flat fibrous structures, including the influence of the melt electrospinning process parameters on the resulting fiber diameter and the porosity and physicochemical parameters of the fibrous structures. The melt electrospinning processing parameters of the tubular structures are shown in Table II.

ANALYTICAL METHODS

Rheological Properties

Melt Mass Flow Rate. Determination of MFR was carried out according to the PN-EN ISO 1133 : 2011 Standard with a TN393LG melt flow indexer (Bexhill on Sea, Germany). The measurements were collected at 170–230°C for PLA and at 180–300°C for PP under a piston loading of 2.16 kg and an inert hole diameter of 2.019 mm. The test sample was filled into preheated measuring chamber. The preconditioning of polymer was taken 6 min, to allow the material to be melt. Then the piston had been pressed sample through the nozzle at the bottom of the test chamber. The samples were cut at equal time intervals and then weighted. At each temperature, 10 measurements for calculation of MFR were collected. The melt flow rates were calculated as follows:

$$MFR = \frac{600 \cdot W}{T};\ \left[\frac{g}{10min}\right] \quad (1)$$

where W is the average mass of the cut-offs; T is the sample cut-off time interval; and 600 is the factor used to convert grams per second into per 10 min (600 s).

The melt flow rate was used to characterize the melt density and was calculated as follows:

Table II. Melt Electrospinning Processing Parameters of the Flat and Tubular Structures

Flat structures

	Melt electrospinning processing parameters			
Type of polymer	Temperature of head (°C)	Optimal twist of screws (rpm)	Distance of collector to spinneret (cm)	Spinning voltage (kV)
Moplen HP 456J PP	300	2	10, 15, or 20	25, 30, or 35
Moplen HP 462R PP	290	1	10, 15, or 20	15, 20, 25, 30, or 35
Borlow HL 504FB PP	280	1	10, 15, 20, or 30	20, 25, 30, 35, 40, or 45
PLA 4060D	170	2	10, 15, or 20	25, 30, or 35
PLA 6201D	200	1	10, 15, 20, 25, or 30	15, 20, 25, 30, 35, or 40

Tubular structures

	Melt electrospinning processing parameters					
	Extruder processing parameters				Collector processing parameters	
Type of polymer	Temperature of head (°C)	Twist of screws (rpm)	Distance of collector to spinneret (cm)	Spinning voltage (kV)	Speed of spindle (rpm)	Speed of oscillation (mm s^{-1})
Moplen HP 462R PP	270, 290, or 300	0.1–1.0	8,10, or 15	30, 35, or 38	11	30
PLA 4060D	170, 190, or 200	0.1–1.0	8, 10, or 15	30, 35, or 37	11	30

$$\rho = \frac{(W/T)}{([A * l]/t)} \quad \left[\frac{g}{cm^3}\right] \tag{2}$$

where W is the average mass of the cut-offs; T is the sample cut-off time-interval; A is the mean of the cross-sectional areas of the cylinder and the piston head; l is the predetermined distance moved by the piston; and t is the total time of measurement.

Physical Properties of Melt Electrospun Flat Fibrous Structures

Scanning Electron Microscopy. A Nova NanoSEM 230 scanning electron microscope (FEI Company, The Netherlands) was used to study the morphology of the obtained fibrous structures.

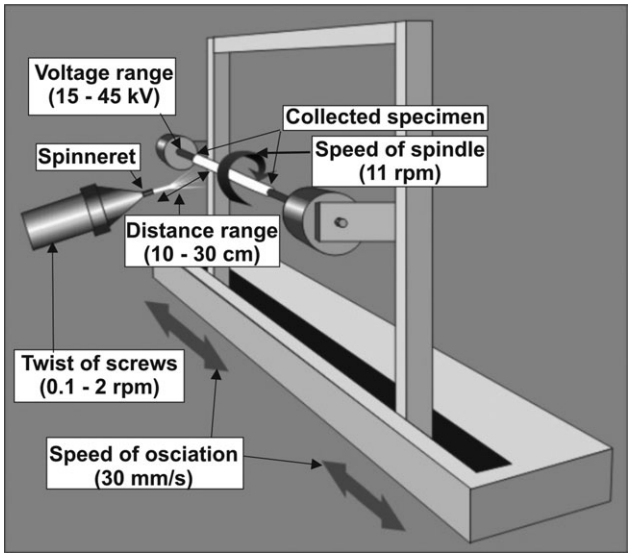

Figure 1. Schematic of the collection device for the fabrication of tubular structures.

Fiber Diameter Determination. For each flat fibrous structure, at least 15 SEM micrographs were taken and 125 fiber diameter measurements were made. The fiber diameter distribution of the melt electrospun fibrous structures was obtained by analyzing the SEM micrographs using Lucia G image-analysis software.

Surface Weight. The surface weight of the fibrous structures was determined according to the PN-EN ISO 29073-1 : 1994 Standard. Ten samples of size 20 × 25 mm were cut out to determine the flat fibrous structures thickness. The measurements were made on the thickness gauge with the pressure sensor DM 12. The sample was charged for 10 s. The flat fibrous structures thickness were determined as an average value of obtained results.

Thickness. The thickness of fibrous structures was determined according to the PN-EN ISO 9073-2 : 2002 Standard. Ten samples of size 20 × 25 mm were cut out to determine the flat fibrous structures surface mass.

Apparent Density and Porosity. The apparent density and porosity characteristics of the electrospun fibrous structures were determined according to the ASTM D2654 : 1998 Standard using the following equations:

$$\text{Apparent density} = \frac{\text{mass of scaffold}}{\text{volume of scaffold}}; \quad \left[\frac{g}{cm^3}\right] \tag{3}$$

$$\text{Porosity} = 1 - \left(\frac{\text{apparent density}}{\text{bulk density of native polymer}}\right); [\%] \tag{4}$$

The bulk density value provided by the polymer manufacturers was 1.24 g cm^{-3} for PLA[17,18] and 0.90 g cm^{-3} for PP.

Applied Polymer SCIENCE

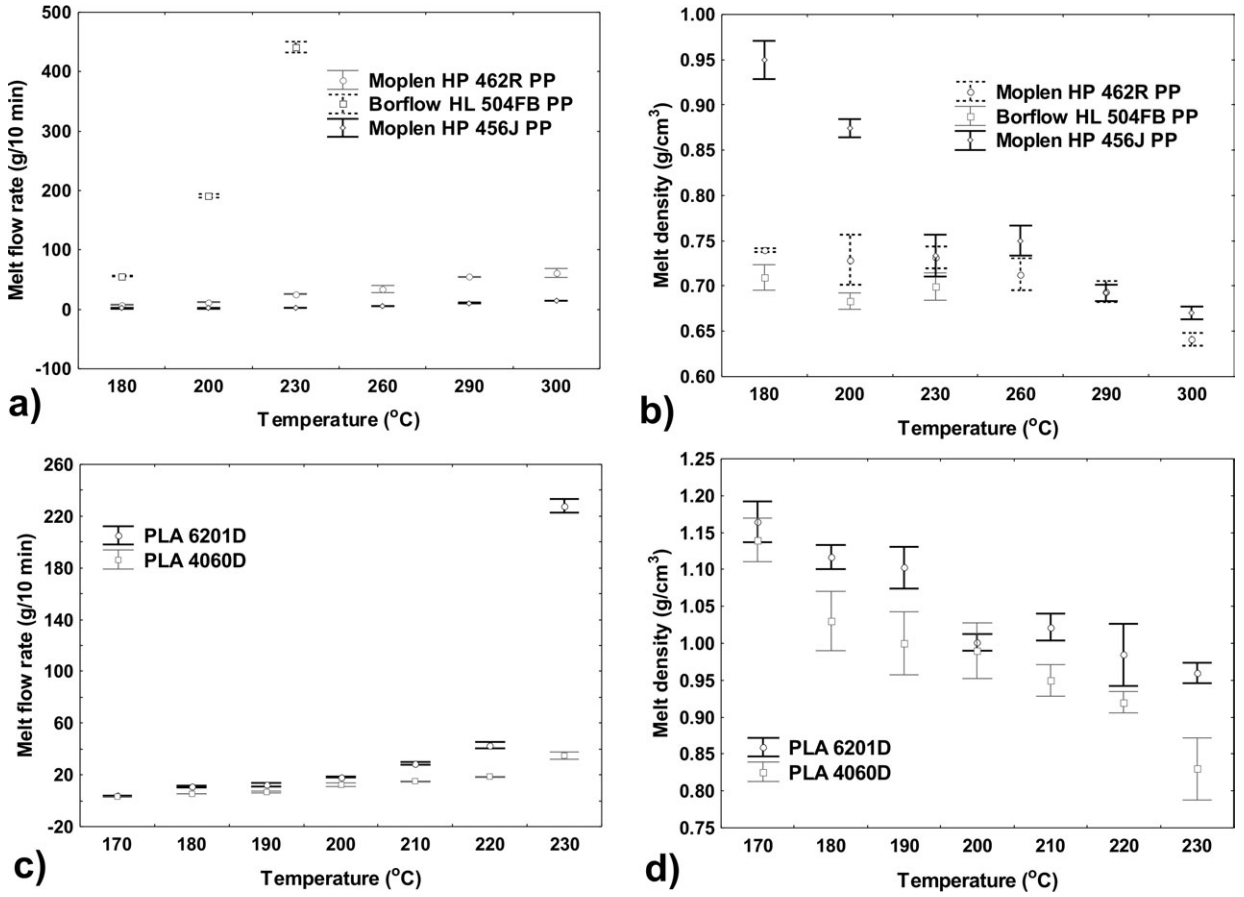

Figure 2. Effect of initial type of polymers and temperature: on the melt flow rate of (a) PP; (c) PLA or on the melt density of (b) PP; (d) PLA.

Structural Properties of Melt Electrospun Flat Fibrous Structures

Differential Scanning Calorimetry. DSC measurements were carried out to determine the thermal characteristics, such as the glass transition temperature (T_g), the cold crystallization temperature (T_c), and the melting temperature (T_m), using a Q2000 device (TA Instruments) that was calibrated with indium. All measurements were made at a heating rate of 10°C min^{-1} over a temperature range of 0–200°C in a dry nitrogen environment according to the PN-EN ISO 11357 : 2009 Standard.

The enthalpy of crystallization up on heating, ΔH_c, and melting, ΔH_m, was measured.

The CI of the samples was calculated using the following equation:

$$\text{Crystallinity index} = \left[\frac{\Delta H_m - \Delta H_c}{\Delta H_f}\right] \cdot 100;[\%] \qquad (5)$$

where

ΔH_f is theoretical heat of fusion of 100% crystalline PLA with a value of 93[19] and 207 J g^{-1} [20] for PP.

The CI values of the melt electrospun samples were compared to the values obtained for the native polymers.

FTIR-ATR. The spectroscopic measurements of the melt electrospun fibrous structures were performed using a Nicolet FTIR Spectrometer with a coupled Attenuated Total Reflectance adapter using "The Thermo Scientific" control unit. The Fourier Transform Infrared Spectroscopy absorption spectra were collected using a ACD/SpecManager within a wavelength range of 4000–600 cm^{-1}.

The melt electrospun nonwoven structures were made of homogenous polymers, without surface modifications, and could therefore be used for the ATR technique. The representative FTIR spectra of the melt electrospun samples were compared to the native polymer FTIR spectra.

Statistical Calculation

Confirmation of Gauss distribution of fiber diameter in flat fibrous structures was done using Shapiro–Wilk test with the level of significance $P < 0.05$. The null hypothesis was that the distribution of fiber diameter is Gauss distribution. The alternative hypothesis assumes that the distribution of fiber diameter for examined samples differed on the Gauss distribution. Verification shows, that null hypothesis must be rejected, thus for statistical analysis of differences between fiber diameters the Kruscal–Wallis test was used. The level of significance was $P < 0.05$. The null hypothesis was that the tested samples are from the same population, whereas the alternative hypothesis assumes

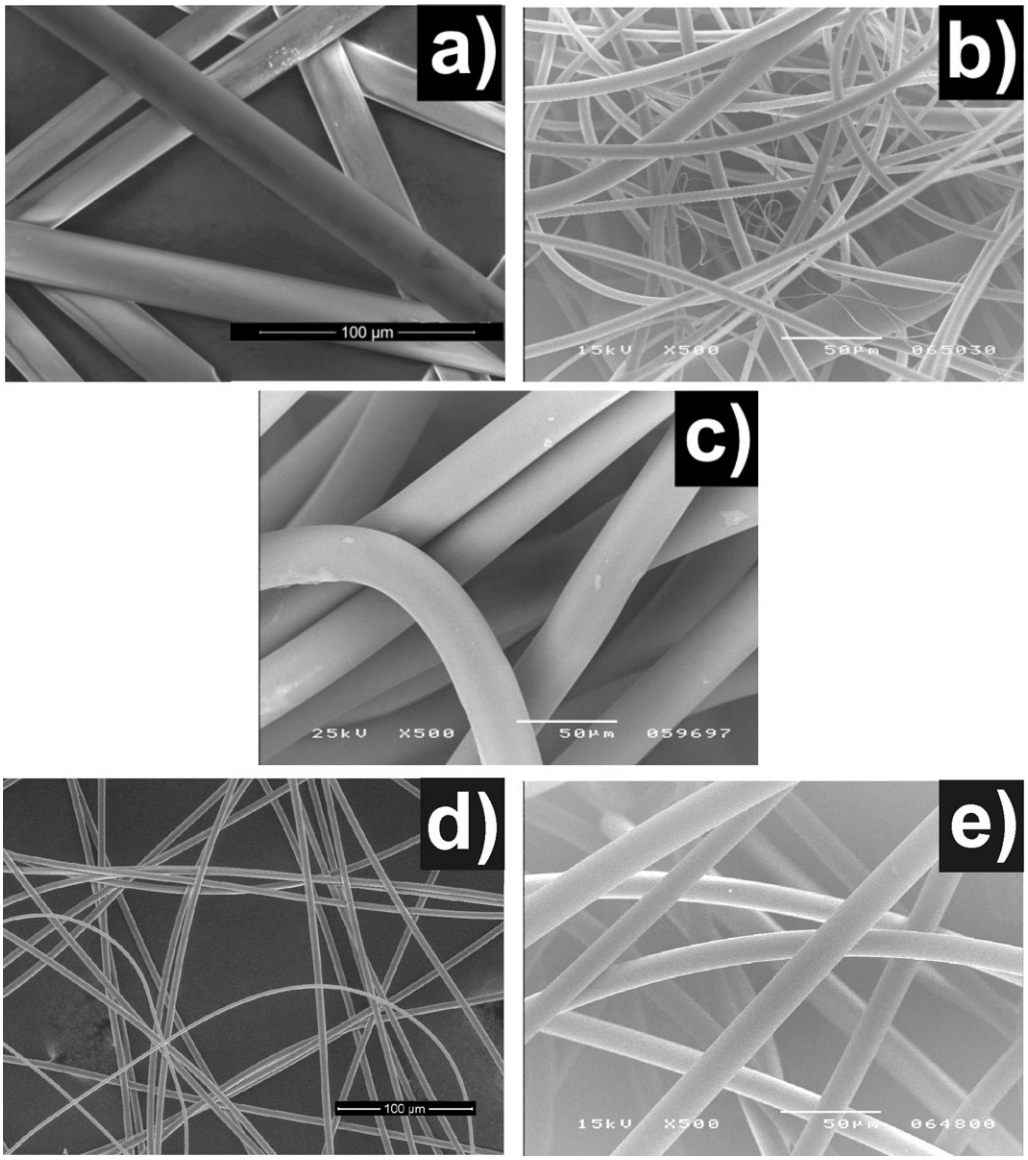

Figure 3. SEM micrographs of the melt electrospun PP or PLA structures for (a) Moplen HP 456J PP deposited at a working distance of 20 cm and at a spinning voltage of 35 kV (magnification 500×); (b) Moplen HP 462R PP deposited at a working distance of 20 cm and at a spinning voltage of 35 kV (magnification 500×); (c) Borflow HL 504FB PP deposited at a working distance of 20 cm and at a spinning voltage of 35 kV (magnification 500×); (d) PLA 4060D deposited at a working distance of 15 cm and a spinning voltage of 35 kV (magnification 800×); (e) PLA 6201D deposited at a working distance of 20 cm and at a spinning voltage of 35 kV (magnification 500×).

that the tested samples are from the different populations. The null hypothesis had been rejected for all cases.

After determination of significant differences between populations of fiber diameter, the Dunn test was used. The level of significance $P < 0.05$ was assumed. The null hypothesis was that the average ranks of fiber diameter are the same. The alternative hypothesis assumes that the average ranks of fiber diameter differ.

RESULTS

Selection of Rheological Properties of Polymers for Melt Electrospinning

Melt Mass Flow Rate. Rheological properties are useful for evaluating thermoplastic performance during processing operations.[21] The MFR tests were prepared for PLA and PP at 180–230°C and 180–300°C, respectively. The test was conducted at various temperatures to determine the optimal temperature for melt electrospinning. Higher temperatures increase the melt flow rate while decreasing the viscosity and melt density. Moreover, the processing temperature should not be significantly high to avoid polymer degradation during the process. Figure 2 shows the effect of the MFR on the temperature of a tested PP specimen under a constant load of 2.16 kg. The lowest melt flow rate for the Moplen HP 456J PP specimen was from 1.7 ± 0.05 to 15.0 ± 0.16 g/10 min at 170–300°C, whereas the highest MFR for the Borflow HL 504FB PP specimen was 43.8 ± 1.34 to 450.0 ± 8.83 g/10 min at 170–230°C, as shown in Figure 2(a). An inverse relationship was observed between the melt

Applied Polymer SCIENCE

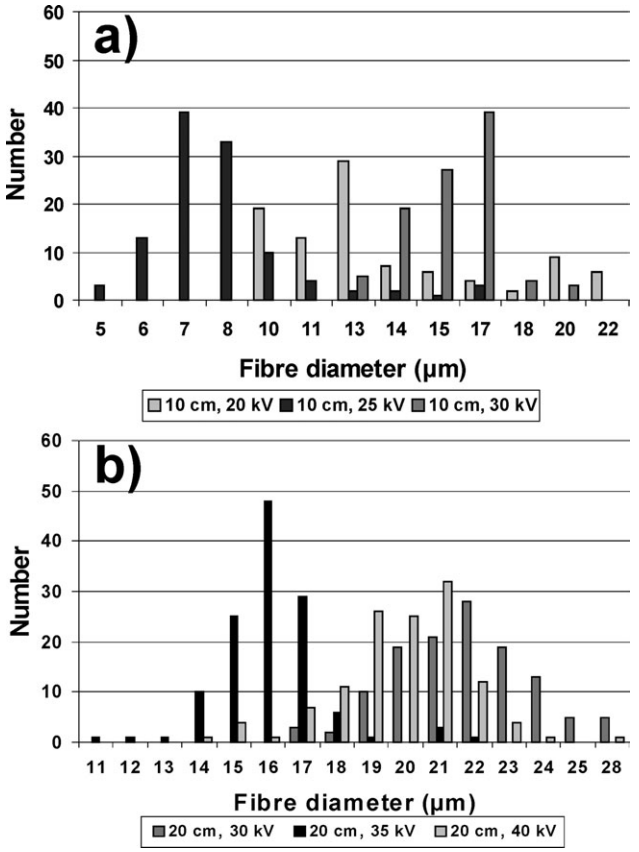

Figure 4. Fiber diameter distribution for (a) the Borflow HL 504FB PP specimen electrospun at a working distance of 10 cm and different spinning voltage and for (b) the PLA 6201D specimen electrospun at a working distance 20 cm and different spinning voltage.

density and the processing temperature, as shown in Figure 2(b). The Borflow HL 504FB PP specimen exhibited the lowest melt density, while the Moplen HP 456J PP specimen showed the highest melt density of the samples tested. It was not possible to determine MFR for the Borflow HL 504FB PP using the TN393LG melt flow indexer at temperatures between 260 and 300°C due to its high melt flow rate. The melted polymer was going too fast by the plastometer's chamber. It was not possible to collect the representative sample.

The interaction forces between the macromolecular chains in the Borflow HL 504FB PP specimen were the weaker than for the Moplen HP 456J PP and the Moplen HP 462R PP. The Borflow HL 504FB PP the flow properties of the melt were improved.[22] The lower MFR of the Moplen HP 456J PP specimen could be the result of its higher molecular weight.[23]

The MFR of the PLA 6201D and PLA 4060D specimens analyzed between 170 and 230°C increased from 4.8 ± 0.37 to 233.0 ± 5.41 g/10 min and from 4.7 ± 0.16 to 41.7 ± 2.81 g/10 min, respectively. However, changes in the MFR of the PLA 4060D specimen were insignificant in comparison to those exhibited by the PLA 6201D specimen.

The results of melt density for the PLA specimen are presented in Figure 2(c). The melt density of the PLA 6201D specimen ranged from 1.11 ± 0.02 to 0.96 ± 0.01 g cm^{-3}, whereas the same parameter for the PLA 4060D specimen was lower, even at the highest temperature (0.83 ± 0.04 g cm^{-3}).The higher melt density of the semicrystalline PLA (PLA 6201D), compared with the amorphous polymer (PLA 4060D), is most likely a result deriving from differences in the polymer molecular structure. An organized structure in the semicrystalline PLA allocates for stronger intermolecular interactions and a relatively higher resistance to flow between the molecules.[24] The number average molecular weight was nearly the same for both the PLA specimens and may not have any influence in the difference between the MFR of the PLA 4060D and PLA 6201D specimens. A comparison of the melt density for both types of PLA at various temperatures is presented in Figure 2(d). Based on the obtained results of the MFR and the melt density, as well as taking into the account the degradation risk limitation, the optimal processing temperature for melt electrospinning was chosen for each polymer specimen:

- PLA 4060D: 170°C;
- PLA 6201D: 200°C;
- Moplen HP 456J PP: 300°C;
- Moplen HP 462R PP: 290°C and
- Borflow HL 504FB PP: 280°C.

Design of Optimal Properties of Melt Electrospun Flat Fibrous Structures

To determine the optimal processing parameters for melt electrospinning, a study for of the three PP and two PLA specimens with different melt flow rates was conducted. The key factors affecting the fiber diameter are the spinning voltage, the distance, and the MFR.

Effect of MFR on Fiber Diameter. Young Lin et al.[25] showed that the influence on the average fiber diameter diminishes in the following order: MFR > voltage > distance > temperature. However, the influence on the fiber diameter standard deviation (SD) occurs in the following order: MFR > temperature > distance > voltage. It is evident that the MFR has significant effect on both the average fiber diameter and the SD.

The lowest fiber diameter for the PP fibrous structures was found for the PP specimen with the medium MFR value, the Moplen HP 462R PP, which was electrospun processed at 20 cm working distance with 35 kV applied voltage. The Moplen HP 456J specimen had the lowest MFR among the PP specimens analyzed in this study, most likely because the applied spinning voltage was not great enough to overcome the polymer viscoelastic forces to generate thinner fibers. The Borflow HL 504FB PP specimen had the highest MFR, resulting in polymer flow that was too fast (rendering it instable) to process through the spinneret extruder and obtain fibers of larger diameter. SEM micrographs of the melt electrospun PP with various MFRs are shown in Figure 3(a–c).

The melt electrospinning process of the PLA was also affected by the MFR. The lowest fiber diameter obtained for the PLA 4060D specimen, even at the lowest processing temperature of 170°C, was smaller than that obtained for the PLA 6201D specimen at 200°C. This phenomenon may be explained by the difference in the molecular structure of the PLA 4060D

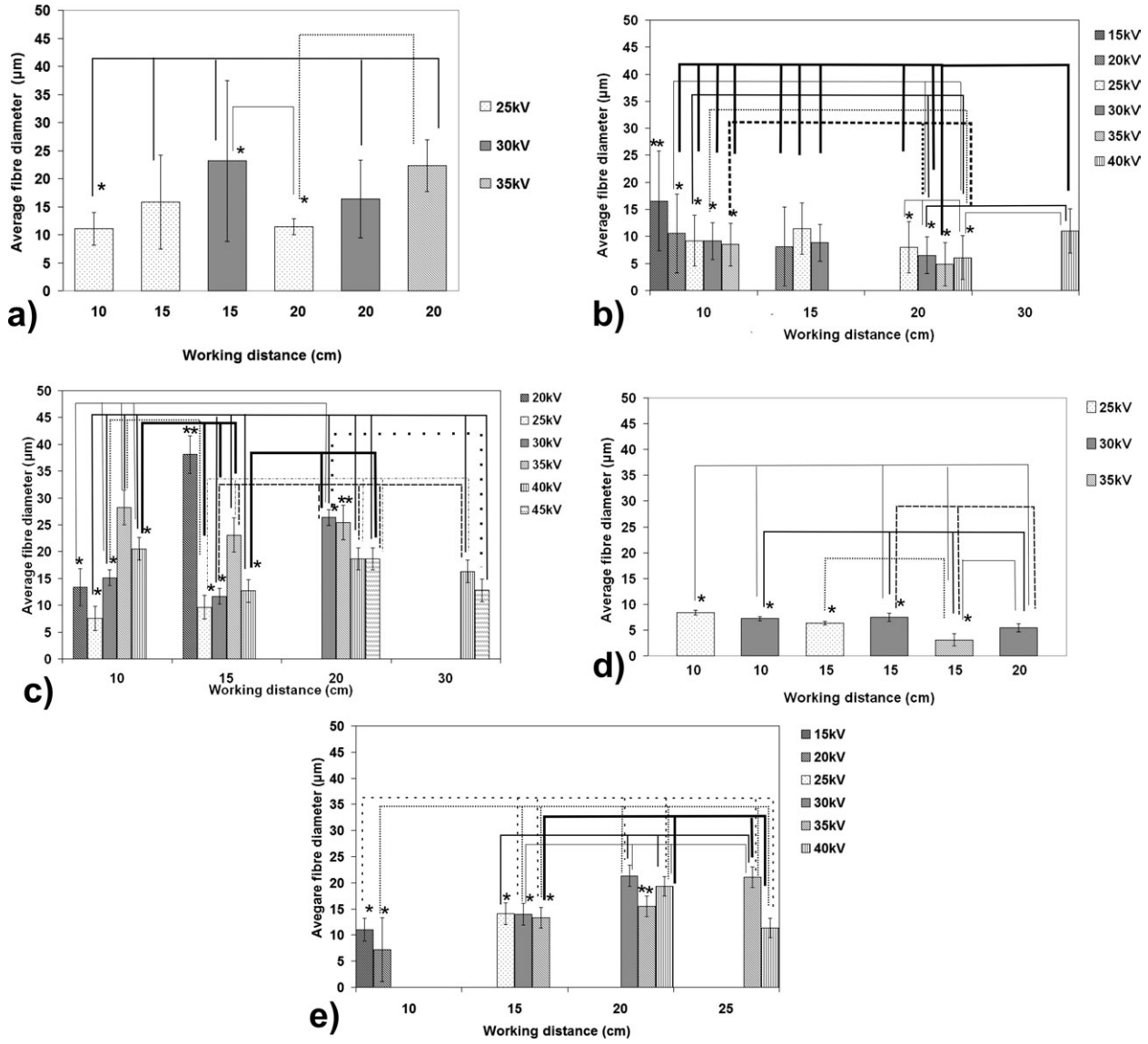

Figure 5. Effect of processing parameters on the average fiber diameter of (a) the Moplen HP 456J PP [15]; (b) the Moplen HP 462R PP; (c) the Borflow HL 504FB PP; (d) the PLA 4060D [15] and (e) the PLA 6201D melt electrospun flat fibrous structures: *significantly statistical difference of mean value (Dunn test; $P < 0.05$); **significantly statistical difference of mean value with all compared samples (Dunn test; $P < 0.05$).

(amorphous) and PLA 6201D (semicrystalline) specimens, and it was also observed directly in terms of the MFR and the fiber diameter. The SD of the PLA 4060D fibers were the lowest of the PLA specimens fabricated. SEM micrographs of the melt electrospun PLA specimens fabricated at various MFR are shown in Figure 3(d,e).

Effect of Working Distance on Fiber Diameter. For the Moplen HP 462R PP specimens, the tendency for forming the lowest fiber diameters was found at a working distance of 20 cm. The fiber diameters of the Moplen HP 462R PP flat samples obtained at aforementioned working distance were varied statistically as compared with other samples manufactured by other applied voltage as well as with the reduction or increase in the melt electrospinning working distance. In other hand, the Moplen 462R PP flat fibrous structures, prepared both at working distance of 10 or 15 cm, were characterized by fiber diameters with no statistical differences among them. The increase in applied voltage above 20 kV at aforementioned working distances did not affect the changes in fiber diameter. The shortened distance between the spinneret and collector can greatly influence the effect of the electromagnetic field on the processed PP specimens by causing reduced fiber elongation, thus resulting in larger diameter fibers. However, the electromagnetic field was less affected by the polymer stream for the experiments conducted at working distance in excess of 20 cm. Such working distances also decreased the fiber diameter. The Borflow HL 504FB PP fibrous structures showed a tendency to form the lowest fiber diameters when they were fabricated at a working distance of 10 or 15 cm and applied voltage of 25 kV. No significant difference between fiber diameters for Moplen HP 456J PP samples was found, if it was formed at working distance of 10

Table III. Physical Properties Melt Electrospun Flat Fibrous Structures of the Moplen HP 456J PP, the Moplen HP 462R PP, the Borflow HL 504FB PP, the PLA 4060D, and the PLA 6201D

Distance between the spinneret and collector (cm)	Spinning voltage (kV)	Surface mass (g m^{-2})	Thickness (mm)	Apparent density (g m^{-3})	Porosity (%)
Moplen HP 456J PP					
10	25	48.42 ± 2.80	0.59 ± 0.02	0.13 ± 0.01	84.84 ± 2.61
10	30	20.94 ± 1.30	0.19 ± 0.04	0.11 ± 0.08	87.07 ± 1.90
15	25	11.65 ± 1.76	0.23 ± 0.09	0.05 ± 0.01	94.37 ± 3.90
15	30	30.51 ± 2.50	0.45 ± 0.08	0.08 ± 0.01	90.49 ± 2.30
15	35	41.07 ± 1.99	0.43 ± 0.06	0.09 ± 0.01	89.38 ± 2.04
20	30	30.51 ± 2.06	0.40 ± 0.05	0.06 ± 0.01	94.49 ± 4.24
Moplen HP 462R PP					
10	20	27.98 ± 2.76	0.45 ± 0.04	0.07 ± 0.01	91.38 ± 2.28
10	30	42.03 ± 4.10	0.28 ± 0.01	0.13 ± 0.04	83.92 ± 4.13
15	25	22.99 ± 2.89	0.19 ± 0.01	0.13 ± 0.02	88.93 ± 2.74
15	30	23.27 ± 3.50	0.25 ± 0.04	0.11 ± 0.02	92.25 ± 1.78
15	35	10.15 ± 2.12	0.30 ± 0.08	0.05 ± 0.01	94.20 ± 1.13
20	30	43.07 ± 2.83	0.41 ± 0.04	0.08 ± 0.01	89.06 ± 1.49
Borflow HL 504 FB PP					
10	25	15.10 ± 3.10	0.44 ± 0.01	0.04 ± 0.01	91.16 ± 2.59
10	30	30.50 ± 6.06	0.19 ± 0.04	0.16 ± 0.09	81.69 ± 4.70
15	25	50.00 ± 5.65	0.33 ± 0.16	0.12 ± 0.06	84.39 ± 3.68
15	30	75.30 ± 4.50	0.70 ± 0.20	0.09 ± 0.02	88.76 ± 3.17
15	35	23.60 ± 1.60	0.19 ± 0.08	0.18 ± 0.07	90.43 ± 2.21
20	30	116.20 ± 16.7	0.80 ± 0.04	0.14 ± 0.06	85.39 ± 3.69
PLA 4060D					
10	25	10.31 ± 1.59	0.03 ± 0.01	0.27 ± 0.10	77.9 ± 4.04
10	30	37.50 ± 9.02	0.18 ± 0.04	0.21 ± 0.05	82.6 ± 4.30
15	25	27.80 ± 5.05	0.15 ± 0.04	0.17 ± 0.05	86.4 ± 2.43
15	30	23.57 ± 3.73	0.13 ± 0.04	0.19 ± 0.03	85.9 ± 3.99
15	35	52.29 ± 3.97	0.42 ± 0.03	0.13 ± 0.01	86.9 ± 3.38
20	30	39.65 ± 4.82	0.40 ± 0.01	0.11 ± 0.05	91.3 ± 4.08
PLA 6201D					
10	20	111.66 ± 4.48	0.49 ± 0.04	0.26 ± 0.04	82.00 ± 4.07
10	30	Unstable electrospinning process resulted in unstable structure of final product			
15	25	14.89 ± 1.11	0.19 ± 0.06	0.14 ± 0.03	91.00 ± 3.10
15	30	51.43 ± 6.70	0.34 ± 0.06	0.17 ± 0.01	88.00 ± 1.80
15	35	75.50 ± 3.07	0.32 ± 0.02	0.19 ± 0.01	81.20 ± 2.90
20	30	39.65 ± 1.74	0.43 ± 0.14	0.09 ± 0.03	92.30 ± 2.21

or 20 cm, at applied voltage 25 kV. In aforementioned cases, all fibers in prepared structures showed the lowest diameters. Results of statistical analysis of PP fiber diameter are presented in Figure 5(a–c). An increase in the working distance increased the SD of the fibers diameter for all PP specimens.

The fabrication of the PLA specimens at a greater working distance caused the fiber diameters to increase. For PLA 4060D, the optimal distance between the spinneret and the collector was 15 cm and applied voltage 35 kV. The statistical differences in fiber diameter for PLA 4060D flat fibrous structure fabricated at a working distance of 15 cm and applied voltage of 35 kV was found for all compared samples independently on processing parameters changing. The statistical analysis of PLA 6201D flat fibrous structures shows a tendency of forming low fiber diameter, if working distance was smaller than 15 cm and applied voltage lower than 35 kV as well as if working distance was 25 cm, but applied voltage 40 kV. Results of statistical analysis of PLA fiber diameters are shown in Figure 5(d,e).

Effect of Applied Voltage on Fiber Diameter. The influence of the spinning voltage on the fiber diameter distribution of the Borflow HL 504FB PP fibrous structures fabricated at a working distance of 10 cm with an increasing spinning voltage is

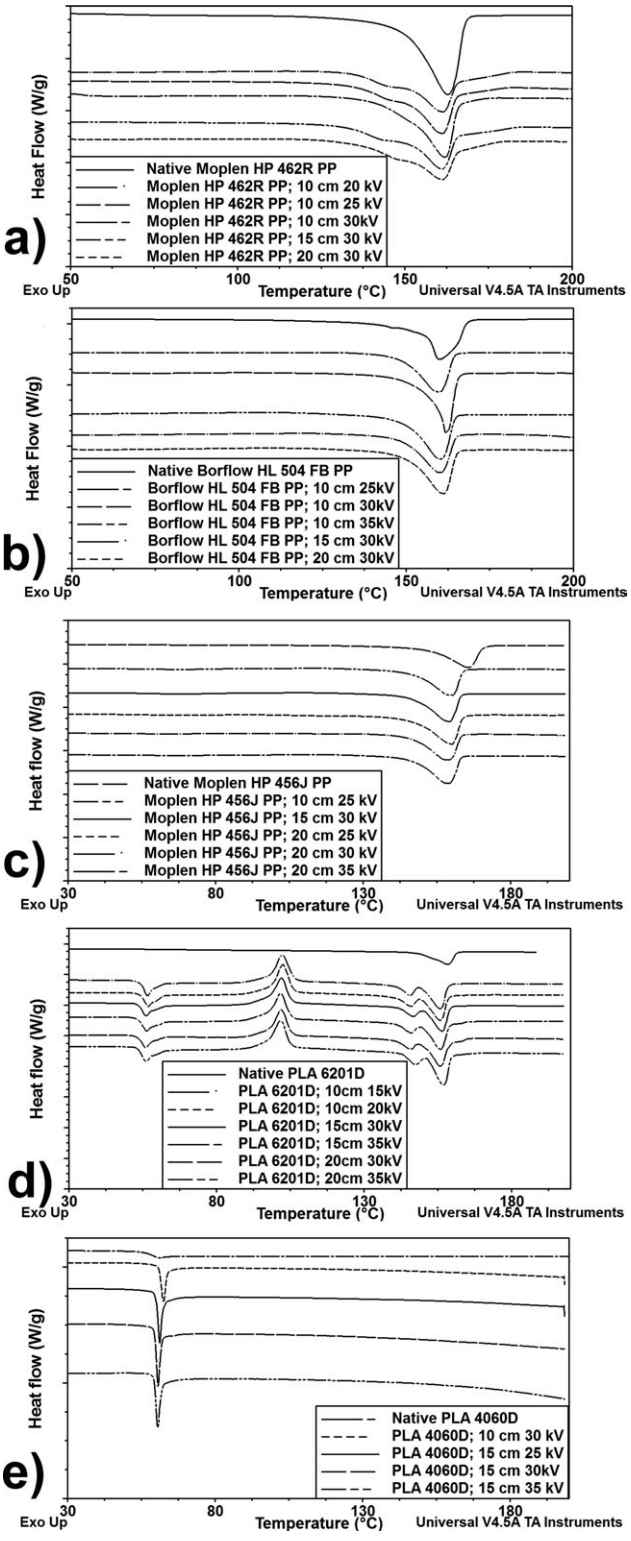

Figure 6. Comparison of the DSC thermographs for the native polymer and flat (2D) structures after melt electrospinning of (a) the Moplen HP 462R PP; (b) the Borflow HL 504FB PP; (c) the Moplen HP 456J PP; (d) the PLA 6201D; (e) the PLA 4060D.

presented in Figure 4(a). For the Borflow HL 504FB and Moplen HP 456J PP specimens, the smallest fiber diameter was observed when fabrication was carried out at 25 kV, as shown in Figure 5(a,c). The increase in the fabrication voltage was not caused by the reduction in fiber diameter. The Moplen HP 462R PP specimen was the only polymer that exhibited its lowest fiber diameter with the application of 35 or 40 kV. The statistical analysis showed that it was not significant difference between samples prepared at working distance 20 cm and applied voltage of 35 or 40 kV. Thus, it is evident that each polymer studied possesses a unique critical voltage. Increasing the voltage causes the Taylor cone to reduce, which subsequently increases the fiber diameter. The smallest fiber diameter is observed when the Taylor cone is present and the jet is formed at the apex of the cone. Increasing the voltage results in a faster pullaway from the polymer fluid that is replaced by the flow rate, which ultimately diminishes the size of the cone.[26–28] The PLA fibrous structures were characterized by the lowest fiber diameter with increasing spinning voltage. The best results were obtained for a spinning voltage of 35 kV, as shown in Figure 4(b).

The flat fibrous structures obtained by melt electrospinning are typically characterized by larger fiber diameters relative to those resulting from electrospinning from solution, but the result depends on the viscosity of the melted polymer.[4–10,25] The effect of the processing parameters on the PP fiber diameters for the flat fibrous structures is presented in Figure 5(a–c). The effect of the working parameters on the fiber diameters for the PLA

Table IV. Crystallinity Index of the Native and Melt Electrospun Flat Fibrous Structures

	Processing parameters		
Polymer used	Distance between the spinneret and collector (cm)	Spinning voltage (kV)	Crystallinity index (CI) (%)
Moplen HP 462 R PP	Native polymer		29.59
	10	20	40.22
	10	25	44.42
	10	30	41.86
	15	30	44.05
	20	30	43.67
Borflow HL 504 FB PP	Native polymer		46.35
	10	25	39.64
	10	30	49.13
	10	35	51.11
	15	30	29.01
	20	30	48.29
Moplen HP 456J PP	Native polymer		41.11
	10	25	44.53
	15	30	41.48
	20	25	45.75
	20	30	40.19
	20	35	44.09

Applied Polymer SCIENCE

Table V. Crystallinity Index of the Native and Melt Electrospun Flat Fibrous Structures

	Processing parameters		
Polymer used	Distance between the spinneret and collector (cm)	Spinning voltage (kV)	Crystallinity index (CI) (%)
PLA 4060D	Native polymer		Amorphous polymer
	10	30	Amorphous polymer
	15	25	Amorphous polymer
	15	30	Amorphous polymer
	15	35	Amorphous polymer
PLA 6201D	Native polymer		2.39
	10	15	4.94
	10	20	6.36
	15	30	5.71
	15	35	12.42
	20	30	18.60
	20	35	13.64

Amorphous polymer: Thermograph does not indicate the melting and cold crystallization peaks.

fibrous flat structures is presented in Figure 5(d,e). The smallest fiber diameter was obtained for the PLA 4060D specimen fabricated at a working distance of 15 cm and an applied voltage of 35 kV.

Physical Properties of the Elaborated Melt Electrospun Flat Fibrous Structures

To be considered for use, implant structures must meet the following selection criteria: (1) exhibit the proper mechanical properties, (2) display suitable porosity for controlled tissue growth, and (3) demonstrate sufficient intrasurgical sealing capability to prevent leaks.[29]

The types of polymer and processing parameters applied during the melt electrospinning process were determined and utilized. The aforementioned parameters greatly influenced the obtained porosity of the fibrous structures.

The Moplen HP 462R PP melt electrospun fibrous structures were characterized with porosity values ranging from 83.92 ± 4.13 to 94.20 ± 1.13%, depending on the processing parameters applied. The porosity values for the Borflow HL 504FB PP melt electrospun fibrous structures ranged from 81.69 ± 4.70 to 91.16 ± 2.59%. The lowest porosity of the melt electrospun structures was observed for the PLA 4060D melt electrospun structures ranged from 77.90 ± 4.04 to 91.3 ± 4.08%; the porosity for the PLA 6201D specimen, ranging from 81.20 ± 2.90 to 92.30 ± 2.21%.

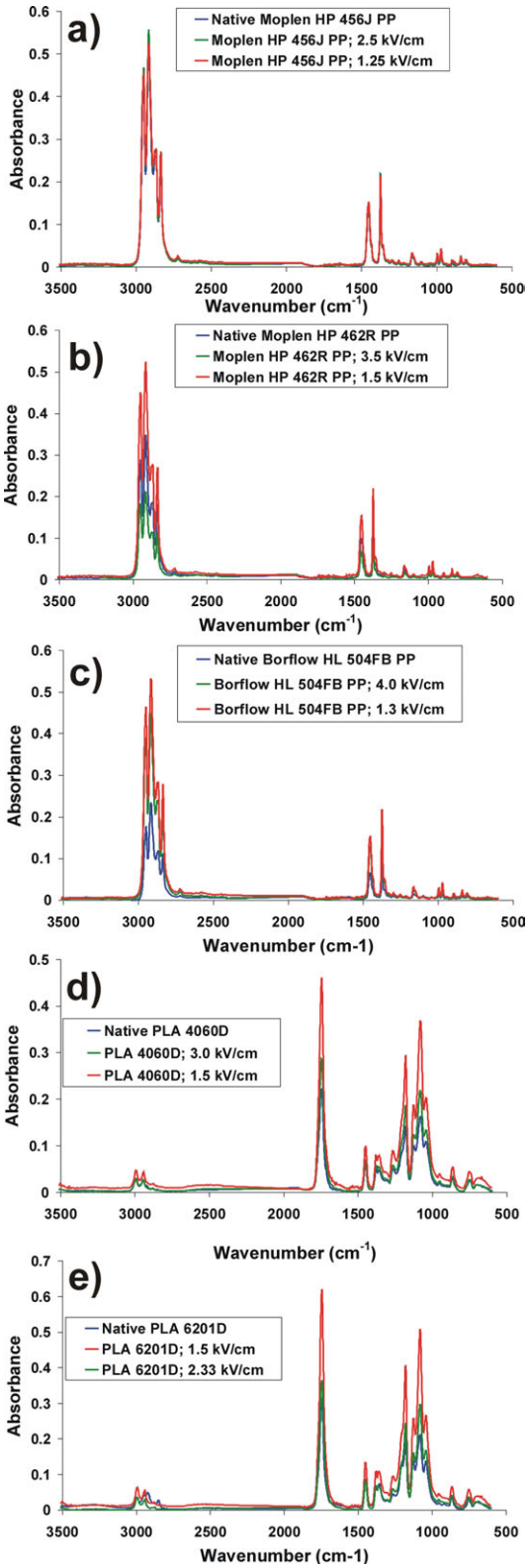

Figure 7. FTIR-ATR spectra of the native and melt electrospun (a) the Moplen HP 456J PP, (b) the Moplen HP 462R PP; (c) the Borflow HL 504FB PP; (d) the PLA 4060D and (e) the PLA 6201D. [Color figure can be viewed in the online issue, which is available at wileyonlinelibrary.com.]

Table VI. FTIR-ATR Peak Assignments for the Native PP and Flat Fibrous Structures After Melt Electrospinning

Wavenumber (cm^{-1}) of separated absorption bands	Vibration type	Assignment
808	Stretching	C—C
840	Rocking	C—H
973	Rocking	CH_3
	Stretching	C—C
996	Rocking	CH_3
1166	Stretching	C—C
	Wagging	C—H
	Rocking	CH_3
1376	Symmetrical bending	CH_3
1456	Symmetrical bending	CH_3
2870	Stretching	CH_3
2920	Asymmetrical stretching	CH_2
2950	Asymmetrical stretching	CH_3

Increasing the working distance decreased the efficiency of the electromagnetic field but had a negligible effect on other forces. Increasing the working distance resulted in structures of greater thickness, lower apparent density, and increased porosity for the obtained melt electrospun structures. The relationships between the PP melt electrospun physical parameters and the processing parameters, where as the dependencies of the PLA fibrous physical parameters on the processing parameters are presented in Tables III.

Structural Properties of the Elaborated Melt Electrospun Flat Fibrous Structures

Differential Scanning Calorimetry. DSC was used to study the changes in the thermal behavior of the melt electrospun flat structures and to compare these structures with the corresponding native polymers. The tests allowed for an analysis of the influence of the melt electrospinning processing parameters based on the thermal properties of the polymer.

The thermal analysis of the native PP shows only major melt endotherm peak at approximately 160°C, without significant changes to the DSC of the melt electrospun fibrous samples prepared under different processing parameters. Changes in the enthalpy of fusion were not observed, indicating that the CI did not change. Figure 6(a–c) shows the DSC thermograph of heat flow as a function of temperature for the PP granulates and the PP melt electrospun structures. The results of the CI for all the PP are listed in Table IV.

The thermograms in Figure 6(e) only show the glass transition (T_g) temperature that is characteristic for amorphous PLA. The native PLA 4060D pellets showed an endothermic peak (relaxation enthalpy) superimposed on the T_g at 57.5°C. The melt electrospun PLA 4060D flat structures also showed an endothermic peak. However, there was no significant increase in the T_g compared to the initial polymer. Table V presents the CI values of the native and melt electrospun PLA 6201D specimens. The thermogram presented in Figure 6(d) for the PLA 6201D specimen shows a glass transition (at ~50°C) and melting peaks (at ~156°C). The melt electrospun structures were additionally characterized by a cold crystallization exothermic reaction (T_c). There were no significant changes in the glass transition peak in comparison with the PLA 6201D native polymer after melt

Table VII. FTIR-ATR Absorption Band Comparison of the Native PP and Melt Electrospun Flat Fibrous Structures

Polymer	Borflow HL 504FB			Moplen HP 462R			Moplen HP 456J		
Melt electrospinning processing parameter: electric field (kV cm^{-1})	Native	4.0	1.3	Native	2.5	1.25	Native	3.5	1.5
Wavenumber (cm^{-1}) of isolated absorption bands	2950	2950	2950	2950	2950	2950	2951	2951	2951
	2917	2917	2917	2917	2917	2917	2917	2917	2917
	2876	2876	2876	2876	2876	2876	2876	2876	2876
	2868	2868	2868	2868	2868	2868	2868	2868	2868
	2837	2837	2837	2837	2837	2837	2837	2837	2837
	2723	2723	2723	2722	2722	2722	2723	2723	2723
	1456	1456	1456	1456	1456	1456	1456	1456	1456
	1376	1376	1376	1376	1376	1376	1376	1376	1376
	1303	1303	1303	1303	1303	1303	1303	1303	1303
	1255	1255	1255	1255	1255	1255	1255	1255	1255
	1167	1167	1167	1167	1167	1167	1167	1167	1167
	997	997	997	997	997	997	997	997	997
	973	973	973	973	973	973	973	973	973
	899	899	899	899	899	899	899	899	899
	841	841	841	842	842	842	842	842	842
	808	808	808	808	808	808	809	809	809

Table VIII. FTIR-ATR Absorption Bands of PLA

Wavenumber (cm^{-1})	Vibration type	Assignment
920		C—O
1044	Stretching	C—CH_3
1080	Stretching	COC
1125	Rocking	CH_3
1265	Stretching and deformation	COC, CH
1356	Deformation and symmetric deformation	CH, CH_3
1380	symmetric deformation	CH_3
1450	Asymmetrical stretching	CH_3
1744	Stretching	C=O
1752	Stretching	C=O
2947	Stretching	CH
2997	Stretching	CH

electrospinning. In the initial heating scan, the DSC curves of the PLA 6201D melt electrospun revealed a multimelting process determined by two separate endotherms. These two endotherms may be explained by the recrystallization behavior of the primary crystallites formed during the cold crystallization process. The difference between the melting peak heat of fusion and the cold crystallization heat of fusion of the PLA 6201D specimen increased due to changes in the melt electrospinning processing parameters and also increased the CI. The CI comparisons for the native and melt electrospun PLA 6201D specimens are shown in Table V.

FTIR-ATR. The FTIR-ATR spectra were collected for the native polymers and the melt electrospun flat fibrous structures (two variants of the melt electrospun flat fibrous structures were fabricated at various melt electrospinning processing parameters: high and low electric field).

Figure 7(a-c) show the FTIR-ATR spectra of the native and melt electrospun PP flat fibrous structures. All the FTIR spectra showed similar absorption bands, which were used to characterise the PP specimens as shown Table VI. Identification of absorption bends was made on base of Hedrick et al.[30] and Abdel-Hamid et al.[31]. The FTIR spectra suggested that the melt electrospinning processing had an insignificant effect on the chemical structure of polypropylene. Table VII presents the FTIR-ATR absorption bands of the initial PP and fabricated flat fibrous structures.

Table VIII presents the characteristic absorption bands for the PLA specimens. Identification of absorption bends was made on base of Meng et al.[32] The polylactide FTIR-ATR spectra were compiled for the native polymers and flat melt electrospun fibrous structures. The selection of the melt electrospun structures was similar to that of the PP. All absorption bands of the native as well as the electrospun PLA 4060D (amorphous) were similar to the presented values in Table IX. Taking this result into account, it can be stated that the melt electrospinning

Table IX. FTIR-ATR Absorption Bands of the Native PLA and Melt Electrospun Flat Fibrous Structures

Polymer used	PLA4060D	PLA 4060D 10 cm; 30 kV	PLA 4060D 20 cm; 30 kV	PLA 6201D	PLA 6201D 15 cm; 35 kV	PLA 6201D 10 cm; 15 kV
Melt electrospinning processing parameter: electric field (kV cm^{-1})	Native	3.0	1.5	Native	2.33	1.5
Wavenumber (cm^{-1}) of the isolated absorption bands	2994	2994	2994	2994	2994	2994
	2945	2945	2945	2945	2945	2945
	-	-	-	2921	-	-
	2879	2879	2879	-	2879	2879
	-	-	-	2850	-	-
	1747	1747	1747	1748	1748	1748
	1453	1453	1453	1453	1452	1452
	1381	1381	1381	1383	1381	1381
	1362	1362	1362	1359	1360	1360
	1319	1319	1319	1305	1307	1307
	1267	1267	1267	1267	1266	1266
	1128	1128	1128	1128	1128	1128
	1044	1044	1044	1043	1043	1043
	956	956	956	956	956	956
	-	-	-	922	-	-
	865	865	865	870	867	867
	753	753	753	755	755	755

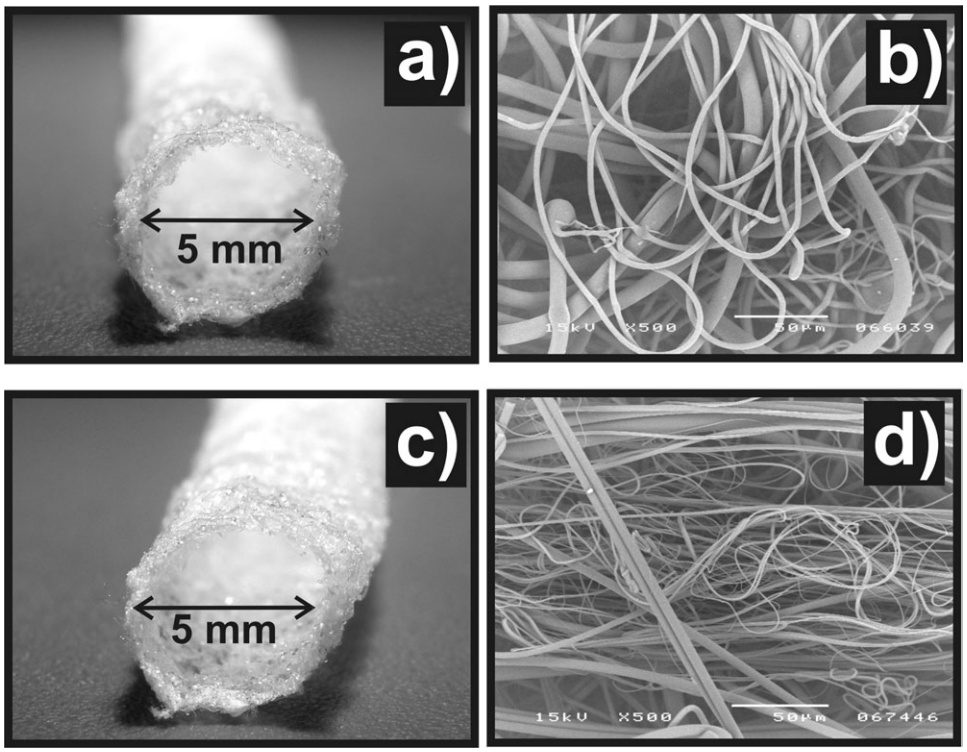

Figure 8. Tubular model made of the Moplen 462R PP or PLA 4060D vascular prosthesis made by the melt electrospinning technique: (a) macroscopic view of tubular model made of the Moplen 462R PP; (b) SEM microphotograph of external surface of tubular model made of the Moplen 462R PP; (c) macroscopic view of tubular model made of the PLA 4060D; (d) SEM microphotograph of external surface of tubular model made of the PLA 4060D.

process does not significantly affect the structure of the PLA polymer. For the PLA 6201D (semicrystalline) specimen, absorption bands at 3000 cm^{-1}-2939 cm^{-1} (—CH stretching), 1759 cm^{-1}-1735 cm^{-1} (—C=O stretching), 1458 cm^{-1} (—CH3 bending) and 1198 cm^{-1}-1185 cm^{-1} (—C—O—C— vibration) are observed. The cold crystallisation band, which was identified for both the PLA melt electrospun flat structures at 1749 cm^{-1}, became more clear and intense. The absorption bands at 2879 cm^{-1}, which are responsible for (—CH) stretching, were not detected for native PLA 6201D but appeared for the melt electrospun structure at 2921 cm^{-1} and 2850 cm^{-1}. However, any absorption peaks at 922 cm^{-1} (—CO—O—) could not be isolated from the FTIR-ATR spectrum for the processed flat structures.[33,34] Table IX presents the FTIR-ATR absorption bands compared with the native polymers of PLA 4060D and PLA 6201D, as well as the melt electrospun flat fibrous structures. Figures 7(d-e) display the FTIR-ATR spectra of the studied samples.

Tubular Structure Design

The next stage of research was the elaboration of three-dimensional (3D; tubular form) straight vascular graft models having inner diameters of 5 mm and less. The special collection device was designed for the elaboration of the 3D fibrous structures and is capable of connecting with high voltage to fabricate fibrous tubular structures by melt electrospinning.

The appropriate polymers for construction of single tubular structures were selected based on the results of flat structure studies, the analysis of the melt electrospinning processing parameters and the influence of the structural and physicochemical properties of the designed flat fibrous structures. The tubular structures of the PLA 4060D were elaborated. The PLA 4060D flat fibrous structures had the highest apparent density with relatively low porosity, which can ensure the intraoperative surgical tightness of the graft. The tubular structures of Moplen HP 462R PP were constructed because the samples were characterized by their large fiber diameter with high reproductively and electrospinning process stability.

The preliminary pictures of the Moplen HP 462R PP and PLA 4060D fabricated tubular structures[30] prepared by melt electrospinning are shown in Figure 8(a,b) and (c,d), respectively. The preliminary results of tubular fibrous structures microscopic observation presented a different distribution of fiber diameter than for flat fibrous structures. The formation of tubular structures on rotating mandrel collector, influence on decreasing of fiber diameter. It will be the basis for future research to determine the factors effecting the changes in the elaborated structures.

CONCLUSIONS

During the initial stage of this study, melt electrospun flat fibrous structures of Moplen HP 456J PP, Moplen HP 462R PP,[15] Borflow HL 504FB PP, PLA 4060D,[15] and PLA 6201 were fabricated. The effects of the MFR and the melt electrospinning processing parameters, such as spinning voltage and working distance between the spinneret and collector, on the final fibrous structures were determined.

It was determined that the MFR has the most significant influence on the resulting structures. Promising results were obtained for Moplen HP 462R PP, which serves as the middle MFR (25 g/10 min at 230°C and 2.16 kg) and for amorphic PLA 4060D. Fibrous structures of the melt electrospun PP with lower or higher MFRs were characterized with a larger average fiber diameter, potentially due to the higher molecular weight of the polymer combined with a low MFR, thus yielding a higher melt density.

An increase in the average fiber diameter for the semicrystalline PLA compared with the amorphic PLA was also observed as the result of stronger intermolecular interactions and a relatively greater resistance to flow.

Finally, the Moplen HP 462R PP specimen was selected as a suitable candidate for the production of melt electrospun 3D structures. The fibrous structures produced from the nonbiodegradable polymer were characterized with the smallest average fiber diameter (4.80 μm) and SD ($\pm$ 4.24 μm) compared to the other PPs examined. In other hands, the PLA 4060D flat fibrous structures demonstrated the appropriate properties for the design of biodegradable layers, as these structures have the lowest average fiber diameter (3.00 μm) and SD ($\pm$1.18 μm). The tubular structures of the PLA 4060D and of the Moplen 462R PP were designed.

ACKNOWLEDGMENTS

The present work is performed within the framework of the project titled "Biodegradable fibrous products" (acronym: Biogratex) supported by the European Regional Development Fund; Agreement No. UDA-POIG.01.03.01-00-007/08-00.

REFERENCES

1. Hoerstrup, S. P.; Zünd, G.; Sodian, R.; Schnell, A. M.; Grünenfelder, J.; Turina, M. I. *Eur. J. Cardiothorac. Surg.* **2001**, *20*, 164.
2. Sarkar, S.; Salacinski, H. J.; Hamilton, G.; Seifalian, A. M. *Eur. J. Vasc. Endovasc. Surg.* **2006**, *31*, 627.
3. Wilson, C. T.; Fisher, E. S.; Welch, H. G.; Siewers, A. E.; Lucas, F. L. *Health Aff. Millwood* **2007**, *26*, 162.
4. Krucińska, I.; Komisarczyk, A.; Chrzanowski, M.; Paluch. D. *Fibres Text. East. Eur.* **2007**, *15*, 5, 73.
5. Błasińska, A.; Krucińska, I.; Chrzanowski, M. *Fibres Text. East. Eur.* **2004**, *12*, 4, 51.
6. Hutmacher, D. W.; Dalton, P. D. *Chem. Asian J.* **2011**, *6*, 44.
7. Klee, K.; Möller, D. *Polymer* **2007**, *48*, 6823.
8. Lyons, J.; Li, Ch.; Ko, F. *Polymer* **2004**, *45*, 7597.
9. Malakhov, S. N.; Khomenko, A. Y.; Belousov, S. I.; Prazdnichnyi, A. M.; Chvalun, S. N.; Shepelev, A. D.; Budyka, A. K. *Fibre Chem.* **2009**, *41*, 355.
10. Larrondo, L.; Manley, S. J. *J. Polym. Sci.: Polym. Phys. Edn.* **1981**, *19*, 909.
11. Kim, J. S.; Jang, D. H.; Park, W. H.; Min, B. M. *Polymer 2010*, **51**, 1320.
12. Chung, S.; Ingle, N. P.; Montero, G. A.; Kim, S. H.; King, M. W. *Acta Biomater.* **2010**, *6*, 1958.
13. Brown, T. D.; Slotosch, A.; Thibaudeau, L.; Taubenberger, A.; Loessner, D.; Vaquette, C.; Dalton, P. D.; Hutmacher, D. W. *Biointerphases* **2012**, *7*, 1.
14. Karchin, A.; Simonovsky, F. I.; Ratner, B. D.; Sanders, J. E. *Acta Biomater.* **2011**, *7*, 3277.
15. Mazalevska, O.; Struszczyk, M. H.; Chrzanowski, M.; Krucińska, I. *Fibres Text. East. Eur.* **2011**, *19*, 4, 46.
16. Krucinska, I.; Surma, B.; Chrzanowski, M.; Skrzetuska, E.; Puchalski, M. Textile Research Journal Available at: http://trj.sagepub.com/content/early/2012/09/23/0040517512460293 (accessed October 4, 2012).
17. NatureWorks® PLA Polymer 4060D, For Heat Seal Layer in Coextruded Oriented Films. Available at: http://www.unicgroup.com/upfiles/file01170656427.pdf (accessed May 8, 2012).
18. NatureWorks® PLA Polymer 6201D, Fiber Melt Spinning. Available at: http://www.natureworksllc.com/~/media/Technical_Resources/Technical_Data_Sheets/TechnicalDataSheet_6201D_pdf.pdf (accessed May 8, 2012).
19. Fischer, E. W.; Sterzel, H. J.; Wegner, G. *Kolloid-Zu Z-Polym.* **1973**, *251*, 980.
20. Cheng, S. Z.D.; Janimak, J. J.; Zhang, A. Q.; Hsieh, E. T. *Polymer* **1991**, *32*, 648.
21. Henton, D. E.; Gruber, P.; Lunt, J.; Randall, J. In Natural Fibers, Biopolymers, and Biocomposites; Mohanty, A. K.; Mistra, M.; Drzal, L. T., Eds.; Taylor & Francis Group: New York, **2005**; Chapter 16, p 542.
22. Liang, J. Z.; Tang, C. Y.; Zhou, L.; He, L.; Tsui, C. P. *Compos. B* **2011**, 1897.
23. Griff, A. L. Melt Index Mysteries Unmasked. Film Lines. http://www.griffex.com/Griff-meltindex.pdf (accessed May 11, 2012).
24. Qi, F.; Milford, A. H. *Ind. Crop. Prod.* **1999**, *10*, 47.
25. Liu, Y.; Deng, R.; Hao, M.; Yan, H.; Yang, W. *Polym. Eng. Sci.* **2010**, 2074.
26. Lyons, J.; Ko, F. *Polym. News* **2005**, *30*, 170.
27. Cengiz, F.; Krucińska, I.; Gliścińska, E.; Chrzanowski, M.; Goktepe, F. *Fibres Text. East. Eur.* **2009**, *17*, 1, 13.
28. Krucińska, I.; Komisarczyk, A.; Chrzanowski, M.; Gliścińska, E.; Wrzosek, H. *Fibres Text. East. Eur.* **2009**, *17*, 3, 38.
29. Lannutti, J.; Reneker, D.; Ma, T.; Tomasko, D.; Farson, D. *Sci. Eng.* **2007**, *27*, 504.
30. Hedrick, S. A.; Chuang, S. S. C. *Thermochim. Acta* **1998**, *315*, 159.
31. Abdel-Hamid, H. M. *Solid-State Electron.* **2005**, *49*, 1163.
32. Meng, Z. X.; Wang, Y. S.; Ma, C.; Zhng, W.; Li, L.; Zheng, Y. F. *Mater. Sci. Eng.: C.* **2010**, *30*, 1204.
33. Goncalves, C. M. B.; Coutinho, J. A. P.; Marrucho, I. M. Poly(lactic acid), Synthesis, Structures, Properties, Processing, and Applications, Auras, R.; Lim, L.; Selke, S. E. M.; Tsuji, H. Wiley: Hoboken, **2010**, Chapter 8, p 97.
34. Pan, P.; Zhu, B.; Kai, W.; Dong, T.; Inoue, Y. *J. Appl. Polym. Sci.* **2007**, *107*, 54.
35. Krucinska, I.; Struszczyk, M. H.; Mazalevska, O. Patent application RP No. P398860, April 17, **2012**.